Carbohydrate Polymers 107 (2014) 16–24

Contents lists available at ScienceDirect

Carbohydrate Polymers

journal homepage: www.elsevier.com/locate/carbpol

Multifunctional PLA–PHB/cellulose nanocrystal films: Processing, structural and thermal properties

M.P. Arrieta[a,e], E. Fortunati[b,*], F. Dominici[b], E. Rayón[c], J. López[a], J.M. Kenny[b,d]

[a] Instituto de Tecnología de Materiales, Universitat Politècnica de Valencia, 03801 Alcoy-Alicante, Spain
[b] Materials Engineering Centre, UdR INSTM, NIPLAB, University of Perugia, 05100 Terni, Italy
[c] Instituto de Tecnología de Materiales, Universitat Politècnica de Valencia, E-46022 Valencia, Spain
[d] Institute of Polymer Science and Technology, CSIC, Juan de la Cierva 3, Madrid 28006, Spain
[e] Analytical Chemistry, Nutrition and Food Sciences Department, University of Alicante, P.O. Box 99, E-03080 Alicante, Spain

ARTICLE INFO

Article history:
Received 28 December 2013
Received in revised form 6 February 2014
Accepted 8 February 2014
Available online 22 February 2014

Keywords:
Poly(lactic acid)
Poly(hydroxybutyrate)
Cellulose nanocrystals
Blends
Nanocomposites
Film processing
Thermal properties

ABSTRACT

Cellulose nanocrystals (CNCs) synthesized from microcrystalline cellulose by acid hydrolysis were added into poly(lactic acid)–poly(hydroxybutyrate) (PLA–PHB) blends to improve the final properties of the multifunctional systems. CNC were also modified with a surfactant (CNCs) to increase the interfacial adhesion in the systems maintaining the thermal stability. Firstly, masterbatch pellets were obtained for each formulation to improve the dispersion of the cellulose structures in the PLA–PHB and then nanocomposite films were processed. The thermal stability as well as the morphological and structural properties of nanocomposites was investigated. While PHB increased the PLA crystallinity due to its nucleation effect, well dispersed CNC and CNCs not only increased the crystallinity but also improved the processability, the thermal stability and the interaction between both polymers especially in the case of the modified CNCs based PLA–PHB formulation. Likewise, CNCs were better dispersed in PLA-CNCs and PLA–PHB–CNCs, than CNC.

1. Introduction

Several biodegradable polymers have been investigated during the last few decades as alternatives to non-degradable polymers currently used in film production with particular attention to the food packaging sector (Armentano et al., 2013; Fortunati, Armentano, Iannoni, & Kenny, 2010). In this sense, poly(lactic acid) (PLA) is one of the most attractive biodegradable polymers used in short-term food commodities (Arrieta, Parres, López, & Jiménez, 2013). PLA can be processed by usual thermoplastic technologies such as extrusion, injection molding, sheet extrusion, blow molding, thermoforming and film forming) (Auras, Harte, & Selke, 2004). PLA is a semicrystalline polymer with low softening temperature and therefore it shows glasslike appearance at room temperature. It is being used in the food industry since seeing through the packaging is one of the most important requirements for consumers (Arrieta, López, Ferrándiz, & Peltzer, 2013) and PLA shows high transparency. Unfortunately, so far the use of PLA as film for food packaging is limited because PLA shows high brittleness (Auras, Harte, & Selke, 2004), low heat resistance (Kose & Kondo, 2013) and poor barrier properties (Martino, Jiménez, Ruseckaite, & Avérous, 2011). Interest in reducing PLA inherent brittleness and improving gas barrier properties has led researchers and industries to develop new PLA matrices with increased crystallinity.

Poly(hydroxybutyrate) (PHB) is the best known poly(hydroxyalcanoate) (PHA) synthesized by controlled bacterial fermentation (Zhang & Thomas, 2011). It presents high crystallinity (Calvão et al., 2012); nevertheless, the main drawback of PHB is that it has the melting temperature at about 170–180 °C (Arrieta, López, Hernández, & Rayón, 2014; Malinová & Brožek, 2011), close to the degradation temperature (typically around 270 °C) (Koller, Salerno, Dias, Reiterer, & Braunegg, 2010), showing a small processing window for melt extrusion (Koller, Salerno, Dias, Reiterer, & Braunegg, 2010; Malinová & Brožek, 2011). Thus, PHB processing temperature should be at least 180–190 °C but its thermal degradation takes place very quickly at these temperatures (Erceg, Kovačić, & Klarić, 2005). Nevertheless, the melting temperature of PHB can be lowered far below the thermal decomposition temperature to make this material much easier to process (Corre, Bruzaud, Audic, & Grohens, 2012) through chemical

* Corresponding author. Tel.: +39 0744492921; fax: +39 0744492950.
E-mail address: elena.fortunati@unipg.it (E. Fortunati).

http://dx.doi.org/10.1016/j.carbpol.2014.02.044
0144-8617/

or physical modifications: introducing other structural units into the PHB backbone or blending with another polymer, respectively (Malinová & Brožek, 2011).

Many modifications have been proposed for extending biopolymers applications such as the addition of modifiers, copolymerization or blending. In this sense, blend process is a common and relatively simple approach to tuning the physical and mechanical properties of biopolymers (Bartczak, Galeski, Kowalczuk, Sobota, & Malinowski, 2013). The modification of biopolymers by blending with other bio-based and/or biodegradable polymer has many advantages, because it offers the opportunity to improve properties in a wide range, while legislation also favors completely compostable materials with minimal carbon-footprint (Imre & Pukánszky, 2013).

PLA and PHB present similar melting temperatures, thus they can be blended in the melt state leading to a new biodegradable material that combine the advantages of both polymers. It is expected that PHB crystals increase the crystallinity of PLA (Furukawa et al., 2005; Zhang & Thomas, 2011), as well as PLA can significantly improve the stiffness of PHB (Vogel & Siesler, 2008). It has been reported that the best synergic effect is achieved blending PLA and PHB in 75 wt% and 25 wt% ratio, respectively (Abdelwahab et al., 2012; Arrieta, López, Hernández, & Rayón, 2014; Zhang & Thomas, 2011)

Alternatively, the use of natural reinforcements to improve the mechanical properties of biopolymers for food packaging applications represents a promising method without influencing the transparency (Fortunati, Armentano, Iannoni, et al., 2012; Fortunati et al., 2010). For millennia, natural lignocellulosic basic materials, referring to its main constituent cellulose, hemicelluloses and lignin have been used in the form of wood and plant fibers by number of industries in forest products, paper, textiles, etc. (Brinchi, Cotana, Fortunati, & Kenny, 2013). It is known that the high mechanical and nanomechanical performance of natural materials extracted from the agriculture is conferred by cellulosic hierarchical structures (Rayón, López, & Arrieta, 2013). The second generation of cellulosic based materials, focused in the nanometer scale, are represented by cellulose nanocrystals (CNC), which offer new properties including high biodegradability, better uniformity and durability (Brinchi, Cotana, Fortunati, & Kenny, 2013). Cellulose nanocrystals (CNC) have been successfully incorporated into the PLA matrix by Fortunati and colleagues (Bitinis et al., 2013b; Fortunati, Armentano, Iannoni, et al., 2012; Fortunati, Puglia, Monti, Peponi, et al., 2013; Fortunati, Puglia, Monti, Santulli, et al., 2013) and also into the PHB matrix (Patrício et al., 2013) showing an improvement in the mechanical properties better than other reinforcing materials. The incorporation of CNC into the PLA matrix has shown to improve oxygen barrier properties of PLA (Fortunati, Peltzer, Armentano, Torre, et al., 2012). Therefore they are suitable for food packaging applications. Moreover, the incorporation of CNC allows reducing the amount of biopolymer in the final formulation offering additional advantages such as they are fully renewable and biodegradable, and possess high stiffness and low density. CNC are commonly synthesized from the acid hydrolysis of microcrystalline cellulose (MCC) (Bondeson, Mathew, & Oksman, 2006; Fortunati et al., 2012b). However, the homogeneous dispersion of CNC in PLA matrix is not easy to achieve (Kose & Kondo, 2013) due to its hydrophilic character (Martínez-Sanz et al., 2013). One strategy to favor the CNC dispersion and therefore the final properties of the final formulation is using a surfactant for the CNC surface modification (Fortunati, Armentano, Zhou, et al., 2012).

In this work the innovative combination of PLA-PHB blends reinforced with cellulose nanocrystals were prepared by melt compounding extrusion followed by film forming with the main purpose to produce new biodegradable ternary systems with increased interaction, crystallinity and thermal properties. The main objective is to evaluate the effect of synthesized cellulose nanocrystals (CNC) and surfactant modified cellulose nanocrystals (CNCs) in PLA-PHB blends with the aim of improving PLA–PHB processability and obtaining a fully biodegradable film based on PLA matrix with increased crystallinity intended for food packaging. With this propose, PLA–PHB masterbatches were prepared by melt blending and then CNC and CNCs were added prior to film processing to improve the dispersion of the cellulose nanocrystals in the PLA and PLA–PHB matrices. So, cellulose nanocrystals dispersion during processing and in the obtained nanocomposite films was specifically addressed and discussed. Another issue concerning the development of such systems is the thermal stability due to the cellulose nanocrystals introduction and their modification and/or degradation during processing. Thus isothermal and dynamic thermal studies were also conducted. Moreover, fully morphological and structural characterizations of the obtained nanocomposite films were carried out.

2. Experimental

2.1. Materials

Poly(lactic acid) (PLA 2002D, M_n = 98,000 g mol^{-1}, 4 wt% D-isomer) was supplied by NatureWorks (USA), Poly(hydroxybutyrate) (PHB, under the trade name PHI002) was supplied by NaturePlast (France) and microcrystalline cellulose (MCC, dimensions of 10–15 μm) was purchased from Sigma–Aldrich.

2.2. Nanocrystal synthesis and modification

Cellulose nanocrystal suspension was prepared from 20 g of MCC by acid hydrolysis following the recipe used by Fortunati, Peltzer, Armentano, Torre, et al. (2012) (Fortunati, Armentano, Zhou, et al., 2012). Sulphuric acid hydrolysis was carried out with 64% (w/w) at 45 °C for 30 min with continuous stirring. The solution obtained was diluted in ultrapure water (1:200) and the acid was eliminated by centrifugation; the sediment deposits were then dialyzed until neutral pH. An ion exchange resin was added to the cellulose suspension for 24 h and then was removed by filtration in order to ensure that all ionic materials were removed except the H^+ counter ions associated with the sulfate groups on the CNC surfaces. Ultrasonic treatment was also carried out in a Vibracell 75043, 750 W, Bioblock Scientific for 2 min in an ice bath. Cellulose nanocrystals were also modified by adding STEFAC TM 8170 (Stepan Company Norhfield) surfactant, an acid phosphate ester of ethoxylated nonylphenol, in 1/1 (w/w), and designed as CNCs. The dry content yield was calculated by the determination of dry matter content (W_{dm}) (Eq. (1)) following the oven drying method (UNE-EN ISO, 2008).

$$W_{dm} = \frac{m_1}{m_0} \times 100 \quad (1)$$

where m_0 is the mass content before drying and m_1 is the mass content after drying.

Nanocrystal solutions were neutralized by the addition of 1.0% (w/w) of 0.25 mol l^{-1} NaOH and freeze-drying to obtain a power.

2.3. PLA–PHB blending and nanocomposite preparation

PLA–PHB were blended in 75:25 proportion, according to the literature (Abdelwahab et al., 2012; Arrieta, López, Hernández, & Rayón, 2014; Zhang & Thomas, 2011). Meanwhile, a cellulose nanocrystal content of 5% was selected according with previous results (Fortunati, Armentano, Zhou, et al., 2012). PLA matrix nanocomposites with CNC and CNCs were also produced for

Table 1
PLA and PLA–PHB nanocomposite film formulations.

Materials	PLA (wt%)	PHB (wt%)	CNC (wt%)	CNCs (wt%)
PLA	100			
PLA-CNC	95		5	
PLA-CNCs	95			5
PLA–PHB	75	25		
PLA–PHB-CNC	71.25	23.75	5	
PLA–PHB-CNCs	71.25	23.75		5

comparison. Sample blend formulations and their concentrations are summarized in Table 1.

Nanocomposites were manufactured by using a twin-screw microextruder (DSM explorer 5&15 CC Micro Compounder). It is known that to prevent thermomechanical degradation during the extrusion process, screw speed, mixing time and temperature profile must be carefully selected (Fortunati et al., 2010). Therefore, a screw speed of 150 rpm and mixing time of 3 min were used to optimize the material final properties (Fortunati, Armentano, Iannoni, et al., 2012; Fortunati, Armentano, Zhou, et al., 2012).

In the case of binary PLA and cellulose nanocrystal based systems, PLA pellets, previously dried, were put in the microextruder manually to reach a head force of 1200 N while a temperature profile of mixing process with a maximum temperature of 200 °C with three steps: 180–190–200 °C, was selected. After 2 min, CNC or CNCs were added into the microextruder for 1 additional minute.

In the case of PLA–PHB blends a masterbatch was previously prepared (mixing time of 2 min). PLA–PHB masterbatch was granulated into pellets and then melted in the microextruder (1 min) while CNC or CNCs were subsequently added and mixed during 1 supplementary minute.

Directly after the mixing process, a film forming process with a head force of 3000 N was carried out to obtain PLA and PLA–PHB based nanocomposite films.

2.4. Characterization techniques

2.4.1. Transmission electron microscopy (TEM)

TEM images of cellulose nanocrystals and their nanocomposite films were obtained by Transmission Electron Microscopy (TEM, JEOL JEM-1010) operating at 100 kV. One droplet of CNC or CNCs suspension was deposited on carbon-coated copper grids and dried at room temperature during 20 min before observations.

For the film characterization, they were embedded in epoxy resin and cured during 3 days at room temperature. To observe the cross section, the films were cut with an ultra-microtome (Leica CM1950, SCSIE Universitat de València) and were stained with a uranyl-acetate solution (2 wt%) for about 5 min.

2.4.2. Field emission scanning electron microscope (FESEM)

For the microstructural analysis of the nanocomposite films, the samples were previously frozen in liquid N_2, cryofractured and sputtered with a gold layer. The obtained cross-sections were investigated by FESEM, Supra 25-Zeiss.

2.4.3. Atomic force microscopy (AFM)

AFM analysis was performed to analyze the surface filler dispersion into the polymer matrices. The investigations were carried out by means a Multimode/NanoScope III (Veeco Metrology, Santa Barbara, CA) operating in the tapping mode under air conditions with drive amplitude of 200 mV and an amplitude set point of 1.4 V. Surface roughness was calculated from the AFM topographical images by a Nanoscope Analysis 1.4 software using the root mean square (RMS) parameter.

2.4.4. Thermogravimetric analysis (TGA)

Thermogravimetric measurements were performed in a Seiko Exstar 6300 thermal analyzer. Masterbatch blends were heated under isothermic mode while processed film samples were heated under dynamic mode, both weighing around 5–10 mg. Isothermal tests were carried out at a 200 °C during 40 min under air conditions while dynamic measurements were run from 30 to 900 °C at 10 °C min^{-1} under nitrogen atmosphere.

2.4.5. Differential scanning calorimetry (DSC)

DSC experiments were carried out in a TA Instrument Q200 calorimeter (New Castle, DE, USA). The heating and cooling rate for the scans was 2 °C/min under nitrogen atmosphere with sample weight about 4 mg in hermetic aluminum pans. Calibration was performed using an indium sample. First the cycle program consisted of a heating stage from −25 to 210 °C at a heating rate of 2 °C min^{-1}, followed by a cooling process up to −25 °C and subsequent heating up to 210 °C.

The glass transition temperature (T_g) was taken at the mid-point of heat capacity changes. The melting temperature (T_m) and cold crystallization temperature (T_{cc}) were obtained from the first heating and the degree of crystallinity (χ_c) was calculated through Eq. (2):

$$\chi_c = 100\% \times \left[\frac{\Delta H_m - \Delta H_{cc}}{\Delta H_m^c}\right] \times \frac{1}{W_{PLA}} \quad (2)$$

where ΔH_m is the melting enthalpy, ΔH_{cc} is the cold crystallization enthalpy, ΔH_m^c is the melting heat associated to pure crystalline PLA (93 J g^{-1}) (Turner, Riga, O'Connor, Zhang & Collis, 2004) and W_{PLA} the weightfraction of PLA in the blend.

2.5. X-ray diffraction

The crystalline phases of the nanocomposite films were examined by X-ray diffraction (XRD) equipment (BRUKER AXS D5005, SCSIE Universitat de València). Scanning was performed on square nanocomposite film surfaces (15 mm × 15 mm) mounted in an appropriate sample holder. The patterns for profile fitting were obtained from a diffractometer using Cu K_α radiation with a scanning step of 0.02° between 2.5° and 40° in 2θ with a collection time of 10 s per step, while the voltage was held at 40 kV.

2.5.1. Fourier transformed infrared spectroscopy (FTIR)

FTIR measurements of the nanocomposite films were carried out at room temperature in transmission mode by a Jasco FTIR spectrometer. Spectra were obtained in the 4000–600 cm^{-1} region.

3. Results and discussion

3.1. Cellulose nanocrystal dispersion

CNC and CNCs yield reactions resulted in ca. 20.6 ± 5.3%, in good accordance with previous reported works (Bitinis et al., 2013b; Fortunati, Armentano, Iannoni, et al., 2012; Fortunati, Armentano, Zhou, Puglia, et al., 2012). While pristine CNC suspension reached a constant pH between 8.5 and 9, the pH of CNCs solution after the modification procedure was around 3. Therefore, CNCs solutions were neutralized with NaOH and raised to pH 9 in order to improve the thermal stability of the final nanocrystals.

TEM images of the cellulose nanocrystals obtained (Fig. 1A) show that synthesized CNC (Fig. 1A-a) and CNCs (Fig. 1A-b) exhibit dimensions ranging from 100 to 300 nm in length and between 5 and 10 nm in width confirming previous results (Bitinis et al., 2013b; Fortunati, Armentano, Zhou, et al., 2012).

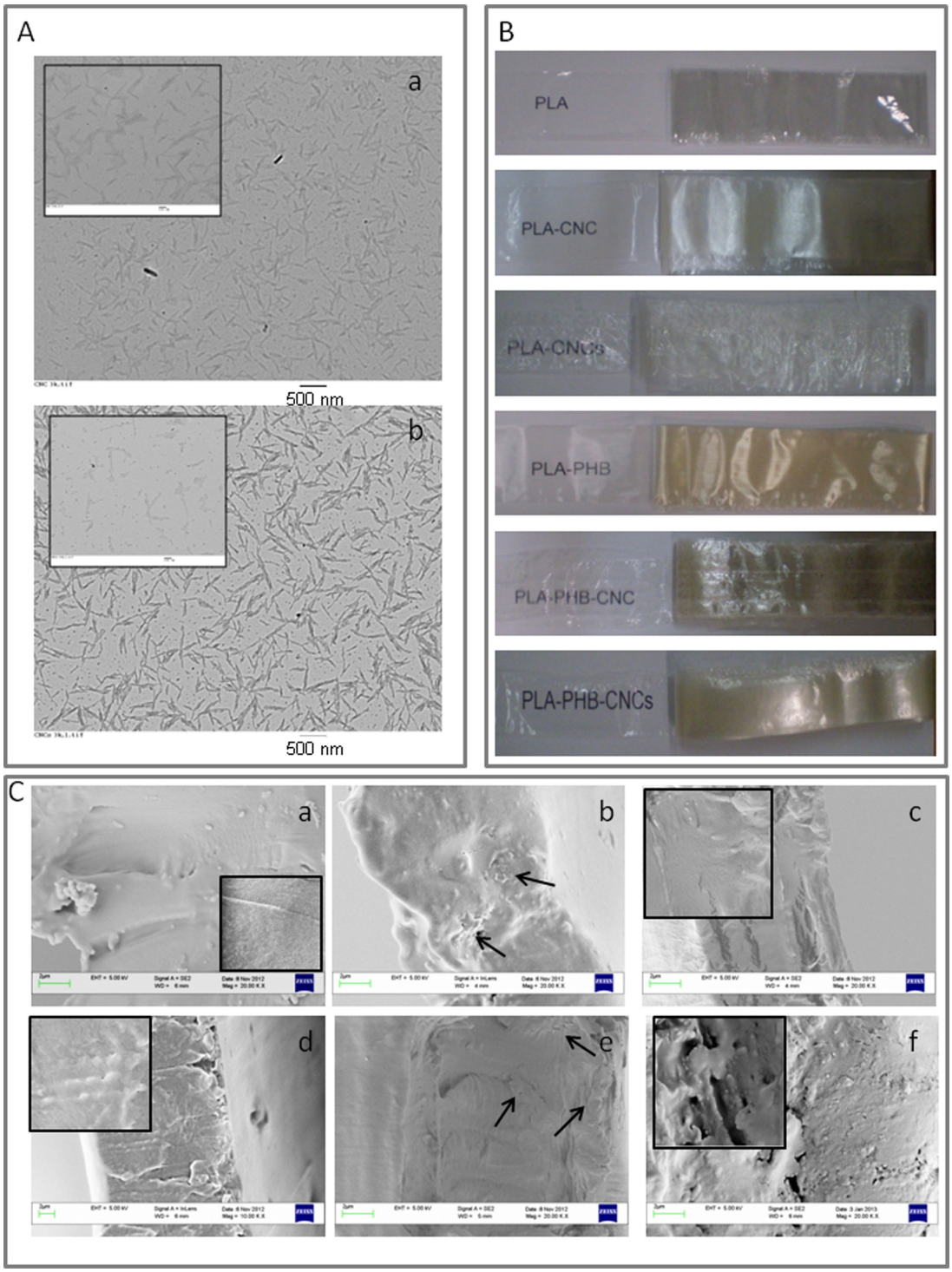

Fig. 1. (A) TEM analysis of (a) CNC and (b) CNCs suspensions. (B) Visual appearance of PLA and PLA–PHB nanocomposite films. (C) Microstructure of fracture surface of (a) PLA, (b) PLA–CNC, (c) PLA–CNCs, (d) PLA–PHB, (e) PLA–PHB–CNC and (f) PLA–PHB–CNCs.

3.2. PLA–PHB-nanocomposite masterbatches and film processing

The use of preformed masterbatches represents a useful technique for industrial end-applications. Therefore, masterbatch processing parameters were studied. During masterbatch processing some changes in the force applied in the system were observed. Neat PLA process started with a 1000 N, but after 1 min the force decreased to around 600 N showing that the material was completely in the melt state. In the case of PLA-PHB masterbatch melting, 30 s after the process, the force notably increased from 1000 N to 1200 N owing to an increase in the viscosity of the system. This behavior was more noticeable in the case of CNC and CNCs based formulations. After the addition of nanoreinforcements the force increased from 1000 N to around 1200 N after CNC incorporation while it increased drastically from 1000 N to around 1400 N with the addition of modified CNCs. This increment in the force was due to the viscosity change that increases with cellulose introduction, showing the effect of nanocrystals on the processing

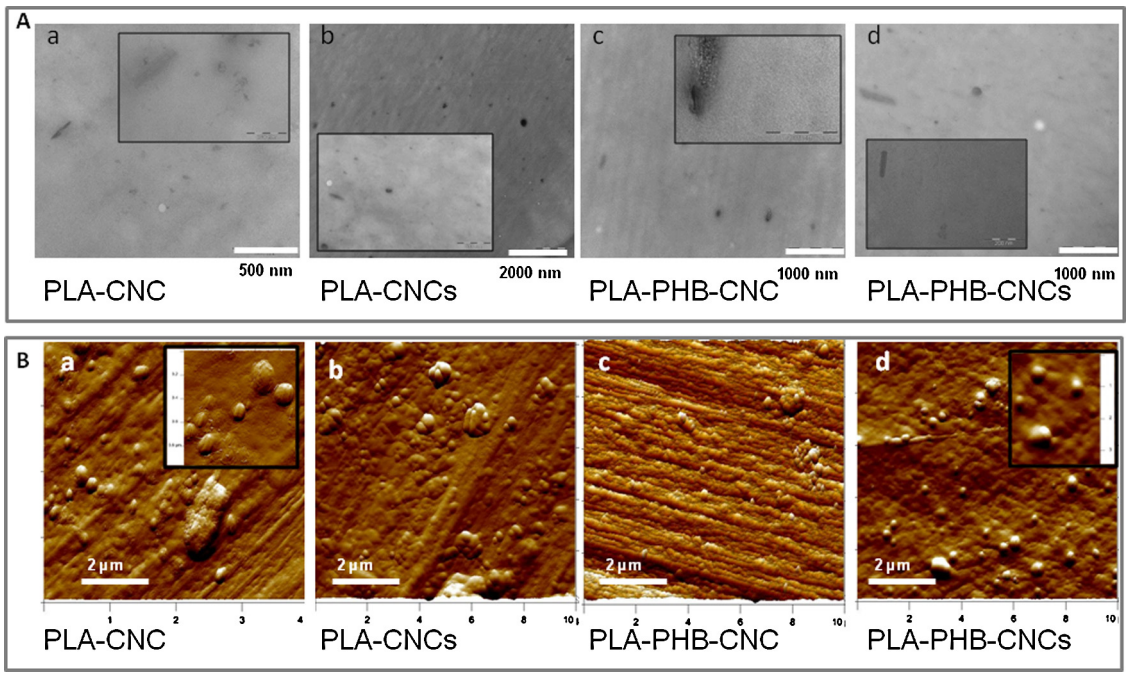

Fig. 2. (A) TEM analysis of nanocomposite films with cellulose nanocrystals: (a) PLA–CNC, (b) PLA–CNCs, (c) PLA–PHB–CNC and (d) PLA–PHB–CNCs. (B) AFM images of nanocomposite films with cellulose nanocrystals incorporated films: (a) PLA–CNC, (b) PLA–CNCs, (c) PLA–PHB–CNC and (d) PLA–PHB–CNCs.

conditions and, consequently, on the final properties of both polymer matrixes.

A similar situation was observed during filming in which the force started at 1200 N, and then it reached a constant value of 400 N and increased to around 600 N in binary PLA–CNC and PLA–CNCs nanocomposite films. While for ternary PLA–PHB formulations the force decreased from 1200 N to around 200 N followed by an increase to around 400 N with CNC and CNCs incorporation during film forming.

3.3. Morphological characterization of the nanocomposite films

PLA and PLA–PHB nanocomposite films with a thickness ranging between 10 and 30 μm are shown in Fig. 1B. It can be noticed when rolling the films that PHB presence produced a tendency to yellow, while CNC or CNCs slightly reduce this trend in PLA–PHB blends. However, all the formulations showed an evident transparency also in the case of PHB based systems, underlining that the presence of 25 wt% of PHB does not affect the PLA original transparency.

Morphological aspects of the cross cryo-fractured sections of pure PLA, PLA–PHB blend, binary and ternary nanocomposite films were investigated by FESEM and the images are shown in Fig. 1C. The pure PLA film (Fig. 1C-a) shows a typical smooth and uniform surface of an amorphous polymer, while PLA–PHB blend (Fig. 1C-d) shows a more toughness surface due of the increased crystallinity. At higher magnification (Fig. 1C-d, insert) PHB particles appear dispersed as crystalline aggregates showing that no phase separation had taken place during the extrusion process. In the case of nanocomposites, CNC based films (Fig. 1C-b and e) show some compact structures (arrows), suggesting that CNC are present in flakes with poor interfacial adhesion (Fortunati, Armentano, Zhou, Puglia, et al., 2012). However, this structure is less pronounced in the PLA–PHB–CNC ternary film (Fig. 1C-e), suggesting that nanocrystals are able to enhance the interfacial adhesion and influence the compatibility between PLA and PHB matrices. Moreover, surfactant modified nanocrystals seem to be better dispersed in both binary PLA–CNCs (Fig. 1C-c) and ternary PLA–PHB–CNCs, (Fig. 1C-f) nanocomposite films, highlighting the positive effect of cellulose modification.

The cellulose structures in the polymer matrices were also studied by transmission electron microscopy (TEM). Individual CNC and CNCs with dimensions ranging from 100 to 300 nm were actually identified in the cross section of the nanocomposite films, confirming the effective incorporation of the synthesized nanocrystals into the polymer matrices (Fig. 2A). It was found that the size of the CNC and CNCs are in agreement with the TEM observations of the cellulose nanocrystal solutions conducted after the hydrolysis procedure (Fig. 1A). Regardless the nanocrystals identification no information on their distribution could be observed by TEM analysis as a result of the low contrast between PLA, PHB and cellulose structures.

Therefore, nanocrystals dispersion was studied by means of AFM analysis on film surfaces in the view of the fact that it represents a more sensitive technique without any limitations concerning contrast and resolution. The phase channel images of the cellulose nanocrystal based films are displayed in Fig. 2B. The unmodified CNC based films showed that the nanocrystals appear somewhat agglomerated (Fig. 2B-a and c), while more individualized structures were detected for CNCs based systems (Fig. 2B-b and d) underlining that the surfactant presence allows the polymer chain penetration between the cellulose structures and confirming SEM and TEM results. Moreover, a topographical analysis was also carried out and it revealed that the RMS value increased from 10.2 nm for PLA-CNC to 49.7 nm for PLA-CNCs. Meanwhile, no significant differences were observed between ternary nanocomposite blend films, which showed RMS values of 14.0 nm for PLA–PHB–CNC and 14.8 nm for PLA–PHB–CNCs. Nevertheless, these differences in roughness surfaces are framed in the nanometer scale.

3.4. Thermal properties of nanocomposite films

The thermal stability of the masterbatches was studied by means of thermogravimetric analysis conducted under isothermal mode at the highest extrusion temperature of 200 °C (Fig. 3a). It was observed that CNC and CNCs slightly improved the thermal stability

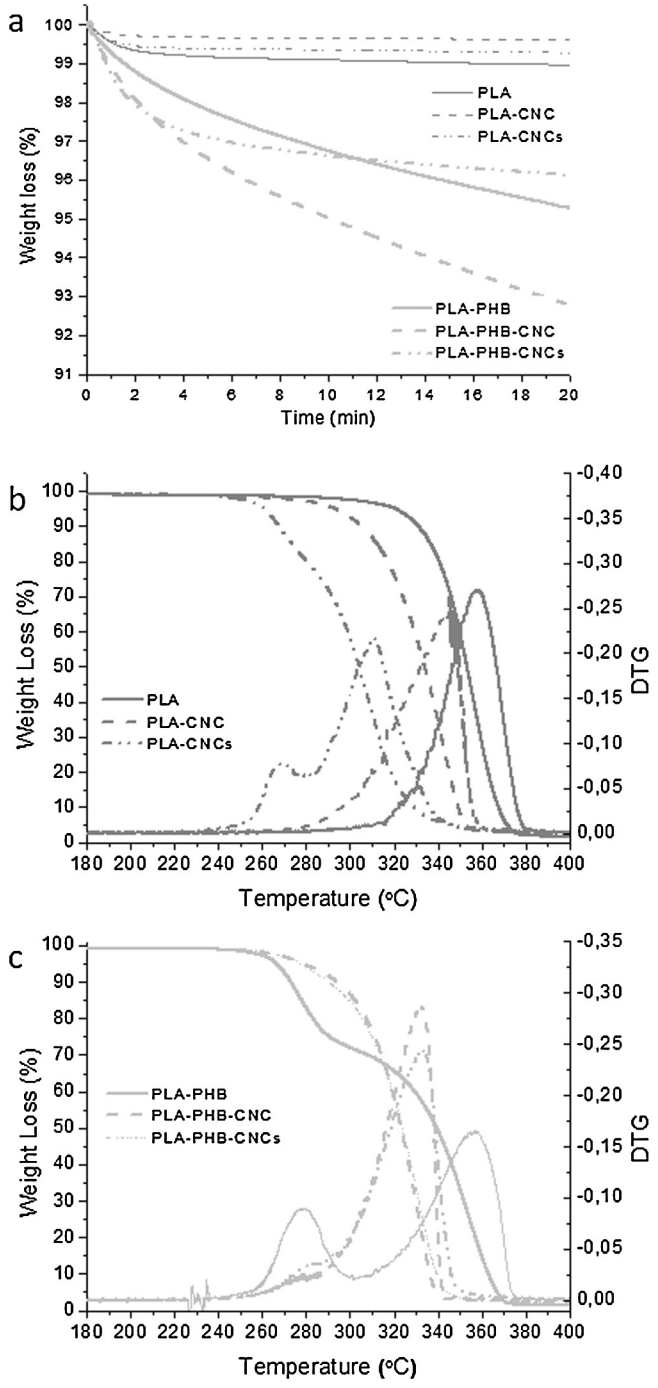

Fig. 3. (a) Isothermal thermogravimetric analysis at 200 °C of binary and ternary masterbatches. (b) Dynamic TGA and DTGA curves of binary PLA nanocomposite films. (c) Dynamic TGA and DTGA curves of ternary PLA–PHB nanocomposite films.

of pure PLA, PLA–CNC and PLA–CNCs losing less than 1% of the initial weight at the processing temperature. Whereas, nanocrystals based PLA–PHB blends showed lesser thermal stability than the neat PLA–PHB blend. It must be noticed that each masterbatch is melt blended using 180–190–200 °C steps as temperature profile during 2 min and subsequently it is inmediately processed into film at 200 °C during no more than 5 min. Thus, after the actual processing time of 7 min at 200 °C, the PLA–PHB–CNC nanocomposite was the lesser thermally stable sample, losing aproximately 5% of the initial mass (Fig. 3a). Meanwhile, sligthly better thermal stability was shown for PLA–PHB–CNCs and PLA–PHB, which presented a mass loss lower than 3%.

The effect of CNC and CNCs on the thermal properties of the PLA–PHB blends was also investigated by dynamic measurements. A one-step degradation process was observed for PLA and PLA–CNC, while PLA–CNCs degraded in two steps (Fig. 3b). In PLA–CNCs the first degradation process, occurring at lower temperatures than the main degradation process, may be related with the loss of the surfactant. PLA–PHB blends and PLA–PHB nanocomposites (PLA–PHB, PLA–PHB–CNC and PLA–PHB–CNCs) degraded in two-steps (Fig. 3c) with the first peak related to the PHB decomposition, and the second peak due to the PLA degradation.

In the binary systems the addition of cellulose fillers shifted the onset of the PLA degradation process toward lower temperatures (Fig. 3b and Table 2). The PLA maximum degradation rate (T_{max}) was also shifted to lower temperatures and with the most evident decrease observed in PLA–CNCs (Table 2). But it must be underlined that there was no degradation at temperatures below 200 °C. As a consequence, PLA integrated with CNC or CNCs were thermally stable at the selected process conditions without risking thermal degradation.

On the other hand, the addition of CNC and CNCs shifted the onset of the PLA–PHB blend degradation process from 266 °C to around 278 °C and led to an improvement in the thermal stability of the ternary nanocomposites. No important changes in the temperature corresponding to the maximum degradation rate of the first stage process ($T_{max\text{-}I}$) were observed (Table 2). However, while the temperature at the maximum degradation rate corresponding to the PLA degradation process was unaffected in the PLA–PHB blend, $T_{max\text{-}II}$ was shifted to lower temperatures (Table 2) in ternary nanocomposites. The changes in the thermal stability due to cellulose nanocrystals introduction lead to enhance the interface interaction between PLA and PHB.

DSC thermal properties obtained for the first heating scan are summarized in Table 2 while DSC thermograms for first and second heating scans are reported in Fig. 4. No significant changes were observed in the glass transition temperature (T_g) between neat PLA and PLA–CNC or PLA–CNCs in good accordance with a previous published work (Fortunati, Armentano, Zhou, et al., 2012). However, a slightly shift to lower T_g values was observed in the PLA–PHB blend while ternary systems showed higher T_g values without significant differences respect to neat PLA. A reduction of PLA cold crystallization temperature was observed in all formulations. The shift of the cold crystallization to lower temperatures in binary PLA–CNC and PLA–CNCs indicates that the addition of cellulose nanocrystals favors PLA recrystallization (Fortunati, Armentano, Zhou, et al., 2012). This behavior was more marked in the case of PHB addition, with a reduction of about 16 °C, showing that PHB crystals act as nucleating agents of the PLA matrix (Zhang & Thomas, 2011). However, a slight shift to higher temperature was observed in the case of ternary PLA–PHB–CNC and PLA–PHB–CNCs with respect to PLA–PHB blend. This increase of almost 5 °C in the cold crystallization could be related to the difference in the flexibility of the chains and their ability to form different crystalline structures (Malinová & Brožek, 2011). Moreover, the degree of crystallinity increased almost 5% in PLA–CNC, PLA–CNCs and PLA–PHB with respect to pure PLA, while in reinforced PLA–PHB it raised up 18.5% for PLA–PHB–CNC and 21.3% for PLA–PHB–CNCs. The higher crystallinity reached by PLA–PHB–CNCs than PLA–PHB–CNC is due to the presence of the surfactant on the nanocrystal surfaces leading to a better dispersion and thus a higher nucleation effect (Fortunati, Armentano, Zhou, et al., 2012). The melting temperatures of the binary and ternary systems do not change significantly with respect to the neat PLA, while the PLA-PHB film shows two peaks in the melting process (Fig. 4c); the first one is due to the PLA component and the second corresponds to the melting of PHB component, suggesting no complete miscibility between the polymers. Conversely, for ternary PLA–PHB–CNC and PLA–PHB–CNCs only one

Table 2
TGA and DSC thermal properties of PLA and PLA–PHB nanocomposite films.

Formulations	TGA parameters			DSC parameters					
	Stage	T_0 (°C)	T_{max} (°C)	T_g (°C)	T_{cc} (°C)	ΔH_{cc} (J g^{-1})	T_m (°C)	ΔH_m (J g^{-1})	χ_c [a] (%)
PLA	–	320	357	58.8	82.5	12.6	149.0	17.7	5.6
PLA-CNC	I	293	343	56.3	74.1	9.7	150.2	20.1	11.7
PLA-CNCs	I	261	267	55.3	78.4	18.9	148.6	28.6	11.0
	II		310						
PLA–PHB	I	266	278	53.5	66.4	19.4	149.6/172.7	28.8	11.9
	II		356						
PLA–PHB-CNC	I	278	280	60.1	70.9	12.8	150.2	25.0	18.5
	II		332						
PLA–PHB-CNCs	I	278	280	62.5	72.1	13.1	148.8	27.2	21.3
	II		333						

T_0, calculated at 5% mass loss (10 °C min^{-1}).
DSC parameters calculated at the first heating scan (2 °C min^{-1}).
[a] χ_c (%), calculated using ΔH_m^c of PLA.

melting peak was observed. This result evidences that well dispersed nanocrystals lead to a clear improvement in the interaction between PLA and PHB.

During the cooling (not shown), no crystallization phenomena were observed for the different formulations and only one deflection due to the glass transition temperature, was observed.

During the second heating scan a double melting behavior, with one peak at around 145 °C and the second one at 151 °C, was observed for PLA, PLA–CNC and PLA–CNCs as it is shown in Fig. 4b ascribed to the formation of small and imperfect crystals that change into more stable crystals through melting and recrystallization at low heating rates or to lamellar populations with two different crystalline phases (Bitinis et al., 2013a). In PLA–PHB blend after the PLA melting peak at around 150 °C two more small melting peaks were present at around 160 °C and 170 °C corresponding to the as-formed PHB crystals during blending process and re-crystallized PHB crystals formed from the re-crystallization during DSC heating, respectively (Zhang & Thomas, 2011). Whereas, PLA–PHB–CNC and PLA–PHB–CNCs films (Fig. 4d) showed a similar behavior to that of the first heating (Fig. 4c). This result is related with the fact that cellulose nanocrystals are small and well dispersed phases able to enhance the interfacial adhesion and consequently improve the compatibility between PLA and PHB matrices. Thus, the melting and re-crystallization of PHB becomes faster than that of PLA–PHB blend in the subsequent heating processes due to CNC and CNCs presence.

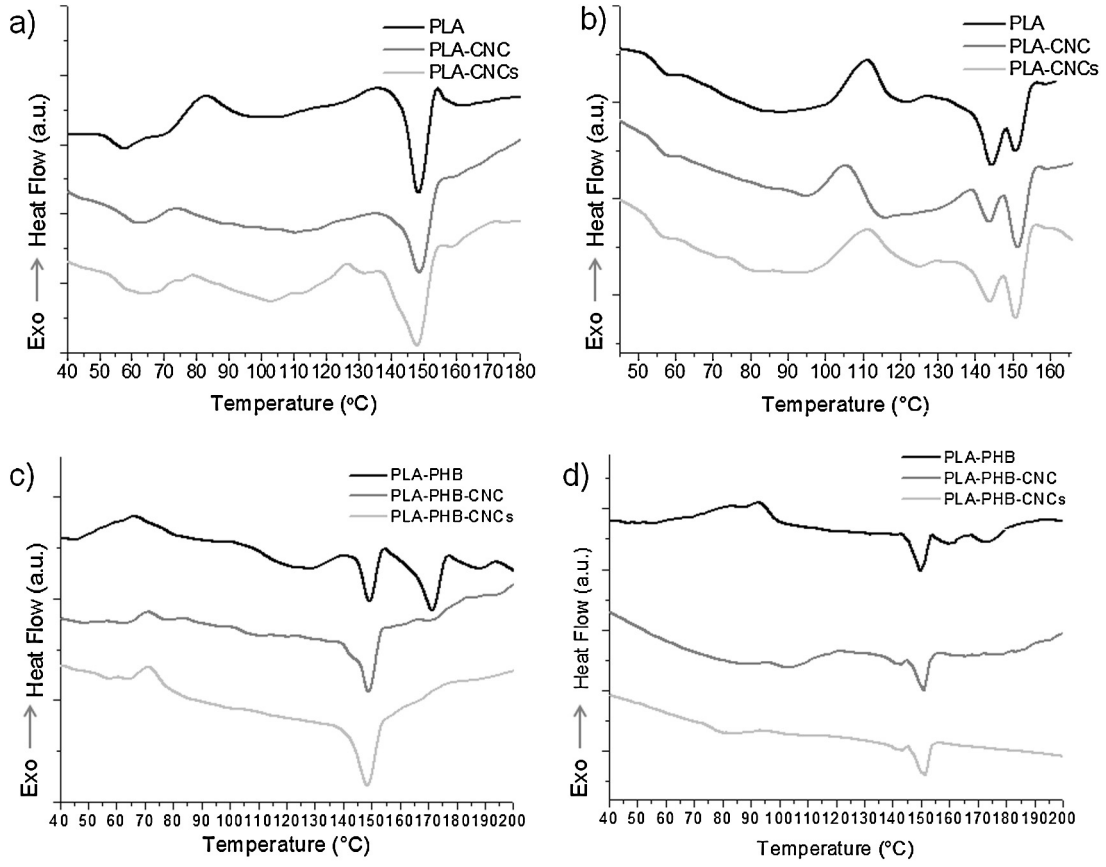

Fig. 4. DSC curves of nanocomposite films during first (a and c) and second (d and e) heating scans.

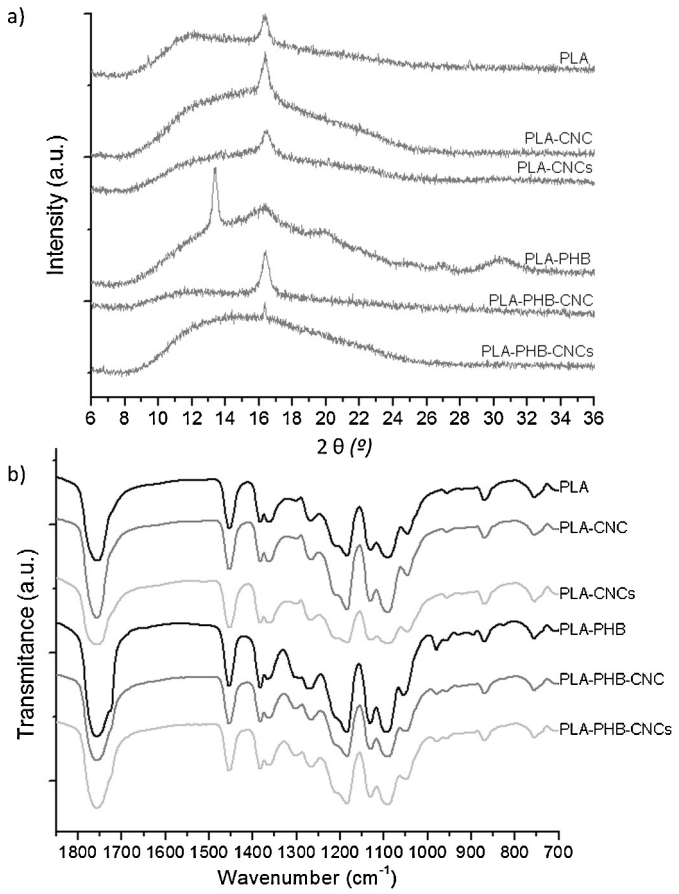

Fig. 5. (a) X-ray diffraction patterns of PLA and PLA–PHB nanocomposite films. (b) Infrared spectra of PLA and PLA–PHB nanocomposite films.

3.5. Structural characterization of nanocomposite films

X-ray diffraction analysis was used to determine the crystalline structure of the nanocomposite films and the results are shown in Fig. 5-a. All films exhibited the characteristic peak of PLA at $2\theta = 16.5^{\circ}$. An increase in the intensity at around $2\theta = 22.5^{\circ}$ is expected for PLA based systems with the CNC (Fortunati, Peltzer, Armentano, Torre, et al., 2012; Hossain et al., 2012) or CNCs (Fortunati, Peltzer, Armentano, Torre, et al., 2012) introduction. However, in this case, this peak was replaced by a broad shoulder in PLA–CNC and PLA–CNCs due to the low cellulose content. PLA–PHB blend exhibited the characteristic peak of PHB at $2\theta = 13.5^{\circ}$ and the peak at $2\theta = 17^{\circ}$ (Abdelwahab et al., 2012; Zhang & Thomas, 2011) was overlapped by the peak at $2\theta = 16.5^{\circ}$ attributed to PLA. PLA–PHB–CNC and PLA–PHB–CNCs ternary systems showed a clearly different XRD pattern respect to the PLA–PHB blend behavior, where the peaks in the $2\theta = 10$–23° range have merged into a single broad peak. The broad X-ray diffraction peaks are indicative of small crystallites size and semi-crystalline character (Turner et al., 2003). In this case, while the broad peak could be influenced by the small cellulose crystal size, the increased intensity at $2\theta = 16.5^{\circ}$ shows that in ternary systems, PLA is re-crystallising confirming, as previous discussed, that the presence of CNC or CNCs is able to positively affect the interaction between PLA and PHB.

Fig. 5b shows the FTIR spectra in the 1900–700 cm^{-1} region. At 1750 cm^{-1} the typical stretching of amorphous carbonyl group (C=O) assigned to lactides was present in all PLA (Auras, Harte, & Selke, 2004) based formulations showing a particularly broad absorption in PLA–PHB blends attributed to the crystalline carbonyl stretching of PHB (Arrieta, López, Hernández, & Rayón, 2014; Phuong Nguyen, Domenek, Guinault, & Sollogoub, 2013; Zhang & Thomas, 2011). This broadening evidences the molecular interaction between both polymers at the selected proportion which has been ascribed to a transesterification reaction between PLA and PHB during melt processing (Zhang & Thomas, 2011). Moreover, PLA–PHB blend shows a shoulder at 1720 cm^{-1} that is replaced by broader bands in PLA–PHB-CNC and PLA–PHB-CNCs. This behavior has been related to the hydrogen interactions between the C=O groups in PHB and —OH groups in CNC (Patrício et al., 2013). The CH deformation and asymmetric bands appear at 1382 cm^{-1} and 1365 cm^{-1}, respectively (Auras et al., 2004). The intensity of the peak at 1382 cm^{-1} increased in PLA-PHB blends spectra due to the CH_3 symmetric deformation of PHB (Furukawa et al., 2005). Moreover, the band at 980 cm^{-1} assigned to the coupling of C—C backbone stretching with the CH_3 stretching vibration band decreases due to CNC and CNCs presence. FTIR spectra showed the miscibility between PLA, PHB and CNC or CNCs, particularly in the ternary systems confirming that CNC and CNCs improve the molecular interaction between PLA–PHB.

4. Conclusions

The study of the blend processing and characterization of the innovative combination of PLA, PHB and cellulose nanocrystals showed the potential of these nanocomposite films for the food packaging industry. Cellulose nanocrystals (CNC) and surfactant modified cellulose nanocrystals (CNCs) were synthesized from microcrystalline cellulose by acid hydrolysis. Synthesized nanocrystals were successfully incorporated in PLA and PLA–PHB blends by preparing a masterbatch prior to the film forming process. The use of a masterbatch improved the dispersion of CNC and CNCs in the final nanocomposite films and made easier the processability between PLA and PHB. CNC and CNCs improved the interfacial adhesion between PLA and PHB and consequently an enhancement of the thermal stability was achieved by shifting the initial degradation temperature of the ternary systems around 10 °C to higher temperatures. This result indicates an improvement of the usually small processing window of the PHB. Thus, PLA, PHB and cellulose nanocrystals can be processed in the region from at least 160 °C and below 200 °C. Moreover, PHB increased the crystallinity of PLA due to its nucleation effect. However, the overall crystallinity was further increased in the PLA–PHB blend by the addition of CNC and this effect was more evident with the addition of modified CNCs, highlighting the positive effect of surfactant modification on the final nucleation process.

The incorporation of surfactant modified cellulose nanocrystals into PLA–PHB blends represents an effective procedure to improve the compatibility between both polymers processed by means of a simple melt-blending process. Moreover, synergic effects in the final properties of ternary nanocomposites are present such as enhanced crystallinity, improved thermal stability and better interfacial adhesion among PLA, PHB and cellulose nanocrystals, showing their suitability for film food packaging industry.

Acknowledgments

This research was supported by the Ministry of Science and Innovation of Spain (MAT2011-28468-C02-01 and MAT2011-28468-C02-02). M.P. Arrieta thanks Generalitat Valenciana (Spain) for Santiago Grisolía Fellowship (GRISOLIA/2011/007) and Universitat Politècnica de València for the Development Support Programme PAID-00-12 (SP20120120).

References

Abdelwahab, M. A., Flynn, A., Chiou, B. S., Imam, S., Orts, W., & Chiellini, E. (2012). Thermal, mechanical and morphological characterization of plasticized PLA–PHB blends. *Polymer Degradation and Stability*, *97*(9), 1822–1828.

Armentano, I., Bitinis, N., Fortunati, E., Mattioli, S., Rescignano, N., Verdejo, R., Lopez-Manchado, M. A., & Kenny, J. M. (2013). Multifunctional nanostructured PLA materials for packaging and tissue engineering. *Progress in Polymer Science*.

Arrieta, M. P., López, J., Ferrándiz, S., & Peltzer, M. A. (2013). Characterization of PLA-limonene blends for food packaging applications. *Polymer Testing*, *32*(4), 760–768.

Arrieta, M. P., López, J., Hernández, A., & Rayón, E. (2014). Ternary PLA–PHB-Limonene blends intended for biodegradable food packaging applications. *European Polymer Journal*, *50*(1), 255–270.

Arrieta, M. P., Parres, F., López, J., & Jiménez, A. (2013). Development of a novel pyrolysis-gas chromatography/mass spectrometry method for the analysis of poly(lactic acid) thermal degradation products. *Journal of Analytical and Applied Pyrolysis*, *101*, 150–155.

Auras, R., Harte, B., & Selke, S. (2004). An overview of polylactides as packaging materials. *Macromolecular Bioscience*, *4*(9), 835–864.

Bartczak, Z., Galeski, A., Kowalczuk, M., Sobota, M., & Malinowski, R. (2013). Tough blends of poly(lactide) and amorphous poly([R,S]-3-hydroxy butyrate) – morphology and properties. *European Polymer Journal*.

Bitinis, N., Fortunati, E., Verdejo, R., Bras, J., Kenny, J. M., Torre, L., & López-Manchado, M. A. (2013). Poly(lactic acid)/natural rubber/cellulose nanocrystal bionanocomposites. Part II: Properties evaluation. *Carbohydrate Polymers*.

Bitinis, N., Verdejo, R., Bras, J., Fortunati, E., Kenny, J. M., Torre, L., & López-Manchado, M. A. (2013). Poly(lactic acid)/natural rubber/cellulose nanocrystal bionanocomposites Part I. Processing and morphology. *Carbohydrate Polymers*.

Bondeson, D., Mathew, A., & Oksman, K. (2006). Optimization of the isolation of nanocrystals from microcrystalline cellulose by acid hydrolysis. *Cellulose*, *13*(2), 171–180.

Brinchi, L., Cotana, F., Fortunati, E., & Kenny, J. M. (2013). Production of nanocrystalline cellulose from lignocellulosic biomass: Technology and applications. *Carbohydrate Polymers*, *94*(1), 154–169.

Calvão, P. S., Chenal, J. M., Gauthier, C., Demarquette, N. R., Bogner, A., & Cavaille, J. Y. (2012). Understanding the mechanical and biodegradation behaviour of poly(hydroxybutyrate)/rubber blends in relation to their morphology. *Polymer International*, *61*(3), 434–441.

Corre, Y. M., Bruzaud, S., Audic, J. L., & Grohens, Y. (2012). Morphology and functional properties of commercial polyhydroxyalkanoates: A comprehensive and comparative study. *Polymer Testing*, *31*(2), 226–235.

Erceg, M., Kovačić, T., & Klarić, I. (2005). Thermal degradation of poly(3-hydroxybutyrate) plasticized with acetyl tributyl citrate. *Polymer Degradation and Stability*, *90*(2 SPEC. ISS.), 313–318.

Fortunati, E., Armentano, I., Iannoni, A., Barbale, M., Zaccheo, S., Scavone, M., Visai, L., & Kenny, J. M. (2012). New multifunctional poly(lactide acid) composites: Mechanical, antibacterial, and degradation properties. *Journal of Applied Polymer Science*, *124*(1), 87–98.

Fortunati, E., Armentano, I., Iannoni, A., & Kenny, J. M. (2010). Development and thermal behaviour of ternary PLA matrix composites. *Polymer Degradation and Stability*, *95*(11), 2200–2206.

Fortunati, E., Armentano, I., Zhou, Q., Iannoni, A., Saino, E., Visai, L., Berglund, L. A., & Kenny, J. M. (2012). Multifunctional bionanocomposite films of poly(lactic acid), cellulose nanocrystals and silver nanoparticles. *Carbohydrate Polymers*, *87*(2), 1596–1605.

Fortunati, E., Armentano, I., Zhou, Q., Puglia, D., Terenzi, A., Berglund, L. A., & Kenny, J. M. (2012). Microstructure and nonisothermal cold crystallization of PLA composites based on silver nanoparticles and nanocrystalline cellulose. *Polymer Degradation and Stability*, *97*(10), 2027–2036.

Fortunati, E., Peltzer, M., Armentano, I., Torre, L., Jiménez, A., & Kenny, J. M. (2012). Effects of modified cellulose nanocrystals on the barrier and migration properties of PLA nano-biocomposites. *Carbohydrate Polymers*, *90*(2), 948–956.

Fortunati, E., Puglia, D., Monti, M., Peponi, L., Santulli, C., Kenny, J. M., & Torre, L. (2013). Extraction of cellulose nanocrystals from Phormium tenax fibres. *Journal of Polymers and the Environment*, *21*(2), 319–328.

Fortunati, E., Puglia, D., Monti, M., Santulli, C., Maniruzzaman, M., & Kenny, J. M. (2013). Cellulose nanocrystals extracted from okra fibers in PVA nanocomposites. *Journal of Applied Polymer Science*, *128*(5), 3220–3230.

Furukawa, T., Sato, H., Murakami, R., Zhang, J., Duan, Y. X., Noda, I., Ochiai, S., & Ozaki, Y. (2005). Structure, dispersibility, and crystallinity of poly(hydroxybutyrate)/poly(L-lactic acid) blends studied by FT-IR microspectroscopy and differential scanning calorimetry. *Macromolecules*, *38*(15), 6445–6454.

Hossain, K. M. Z., Ahmed, I., Parsons, A. J., Scotchford, C. A., Walker, G. S., Thielemans, W., & Rudd, C. D. (2012). Physico-chemical and mechanical properties of nanocomposites prepared using cellulose nanowhiskers and poly(lactic acid). *Journal of Materials Science*, *47*(6), 2675–2686.

Imre, B., & Pukánszky, B. (2013). Compatibilization in bio-based and biodegradable polymer blends. *European Polymer Journal*, *49*(6), 1215–1233.

Koller, M., Salerno, A., Dias, M., Reiterer, A., & Braunegg, G. (2010). Modern biotechnological polymer synthesis: A review. *Food Technology and Biotechnology*, *48*(3), 255–269.

Kose, R., & Kondo, T. (2013). Size effects of cellulose nanofibers for enhancing the crystallization of poly(lactic acid). *Journal of Applied Polymer Science*, *128*(2), 1200–1205.

Malinová, L., & Brožek, J. (2011). Mixtures poly((R)-3-hydroxybutyrate) and poly(L-lactic acid) subjected to DSC. *Journal of Thermal Analysis and Calorimetry*, *103*(2), 653–660.

Martínez-Sanz, M., Abdelwahab, M. A., Lopez-Rubio, A., Lagaron, J. M., Chiellini, E., Williams, T. G., Wood, D. F., Orts, W. J., & Imam, S. H. (2013). Incorporation of poly(glycidylmethacrylate) grafted bacterial cellulose nanowhiskers in poly(lactic acid) nanocomposites: Improved barrier and mechanical properties. *European Polymer Journal*.

Martino, V. P., Jiménez, A., Ruseckaite, R. A., & Avérous, L. (2011). Structure and properties of clay nano-biocomposites based on poly(lactic acid) plasticized with polyadipates. *Polymers for Advanced Technologies*, *22*(12), 2206–2213.

Patrício, P. S. D. O., Pereira, F. V., Dos Santos, M. C., De Souza, P. P., Roa, J. P. B., & Orefice, R. L. (2013). Increasing the elongation at break of polyhydroxybutyrate biopolymer: Effect of cellulose nanowhiskers on mechanical and thermal properties. *Journal of Applied Polymer Science*, *127*(5), 3613–3621.

Phuong Nguyen, T., Domenek, S., Guinault, A., & Sollogoub, C. (2013). Crystallization behavior of poly(lactide)/poly(beta-hydroxybutyrate)/talc composites. *Journal of Applied Polymer Science*, *129*(6), 3355–3365.

Rayón, E., López, J., & Arrieta, M. P. (2013). Mechanical characterization microlaminar structures extracted from cellulosic materials using nanoindentation technique. *Cellulose Chemistry and Technology*, *47*(5–6), 345–351.

Turner, J. F., II, Riga, A., O'Connor, A., Zhang, J., & Collis, J. (2004). Characterization of drawn and undrawn poly-L-lactide films by differential scanning calorimetry. *Journal of Thermal Analysis and Calorimetry*, *75*(1), 257–268.

UNE-EN ISO (2008). Paper, board and pulps - Determination of dry matter content - Oven-drying method (Vol. 638).

Vogel, C., & Siesler, H. W. (2008). Thermal degradation of poly(ε-caprolactone), poly(L-lactic acid) and their blends with poly(3-hydroxy-butyrate) studied by TGA/FT-IR spectroscopy. *Macromolecular Symposia*, *265*(1), 183–194.

Zhang, M., & Thomas, N. L. (2011). Blending polylactic acid with polyhydroxybutyrate: The effect on thermal, mechanical, and biodegradation properties. *Advances in Polymer Technology*, *30*(2), 67–79.